Tuning the Dielectric Response of SnO_2 through Fe-Ce co-doping: Structural and Electrical Insights

Jayshri Narzary

Department of Physics

Bodoland University, Kokrajhar, Assam

Introduction

- SnO_2 is a wide-band-gap, n-type semiconductor with a stable rutile crystal structure and promising electrical, optical and dielectric properties.

- Its chemical stability, low cost and versatile characteristics make it suitable for gas sensors, electronic devices, transparent conducting materials and dielectric applications.

- Its electrical and dielectric properties are influenced by intrinsic defects, grain boundaries, microstructure and charge carriers.

- Doping with transition-metal and rare-earth elements offers an effective approach to tailoring the structural and electrical properties of SnO_2.

- Fe and Ce co-doping may modify lattice distortion, defect chemistry, local crystal environments and charge transport.

- Their incorporation may also influence oxygen-related defects and interfacial polarization, thereby tuning the dielectric response of SnO_2.

Material Preparation by Solid State Reaction route

Composition:

$Sn_{1-x-y}Fe_xCe_yO_2$

x=4% and y=1-4%

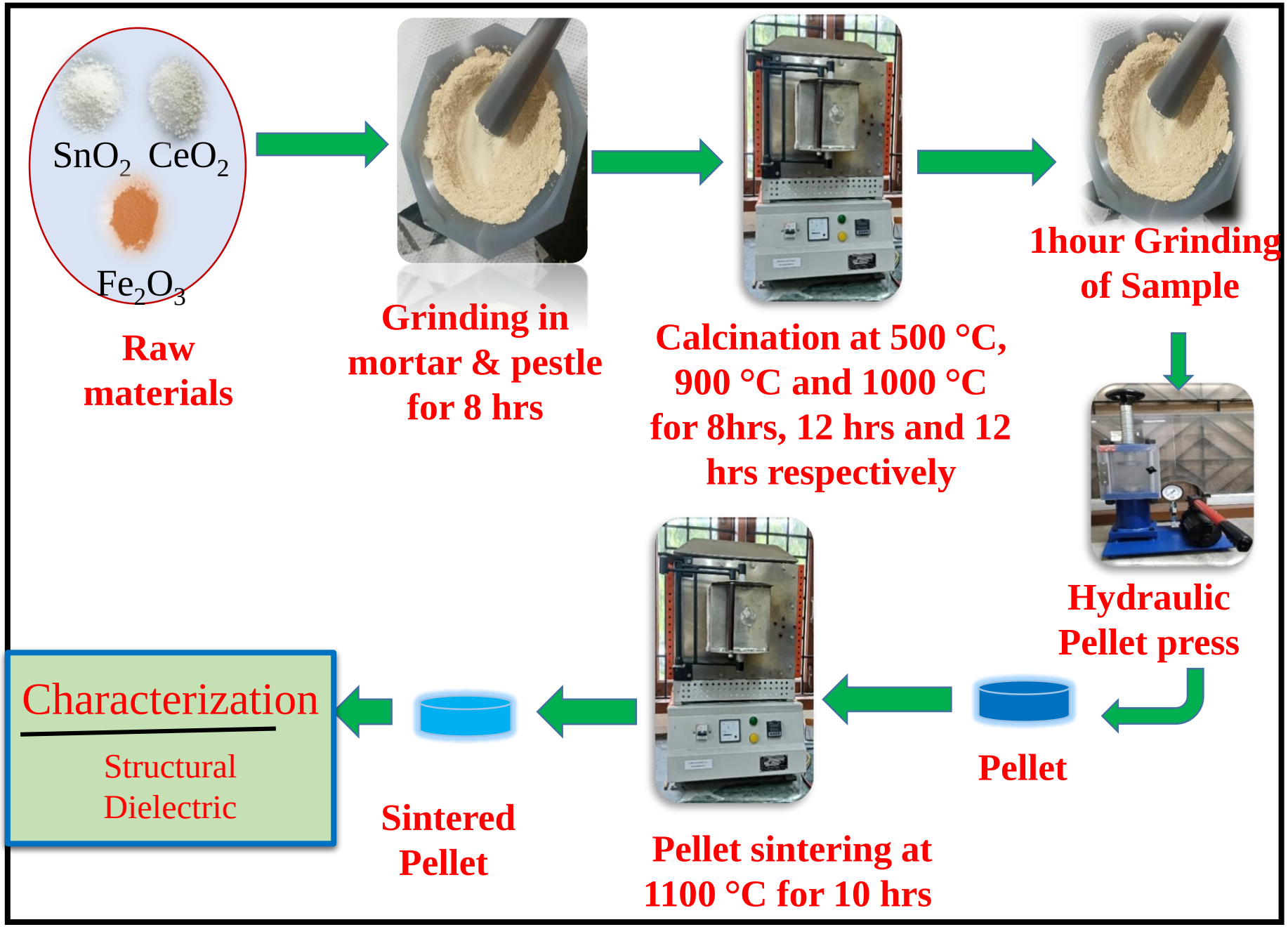

XRD analysis

- tetragonal rutile phase of SnO_2 with space group *$P4_2/mnm$*, consistent with JCPDS Card No. 00-005-0467
- The observed shifting of peaks can be attributed to the substitution of Sn^{4+} (0.69Å)ions by Ce^{3+} (0.87Å)and Fe^{3+} ions (0.76 Å), which possess different ionic radius.
- The average crystallite sizes, estimated using Scherrer's equation range from 21.55 to 24.26 nm

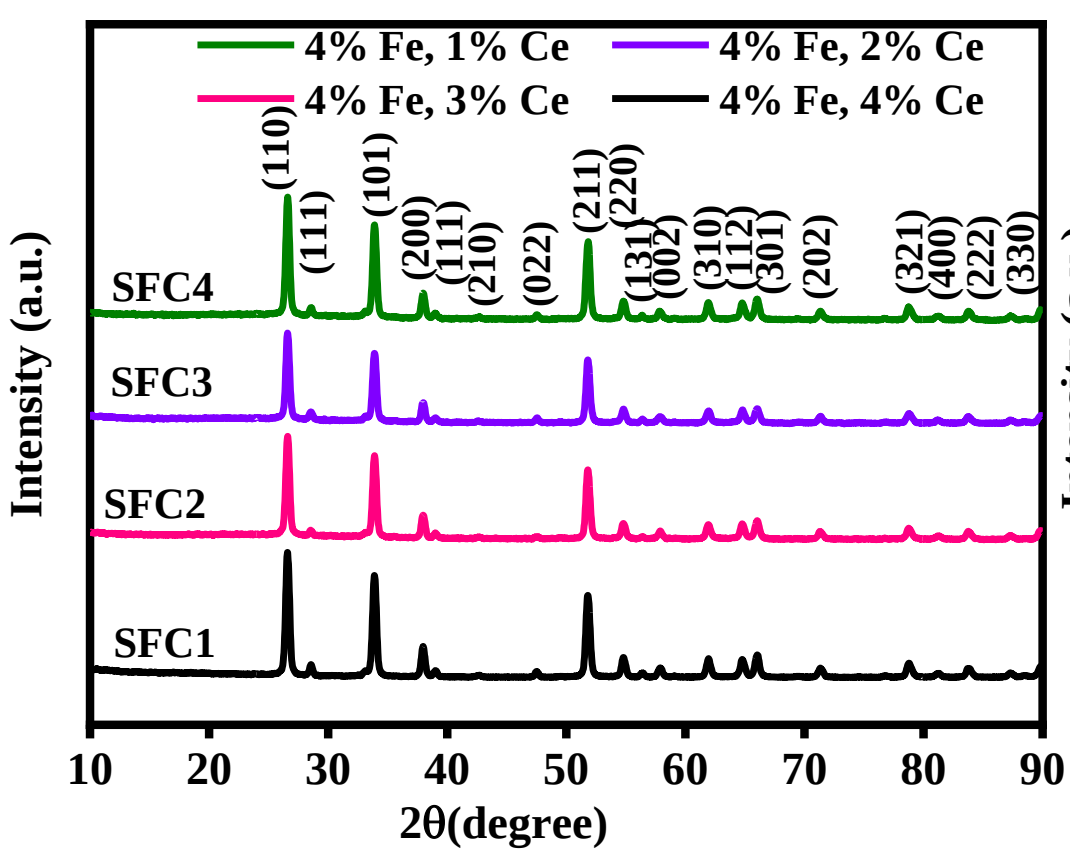

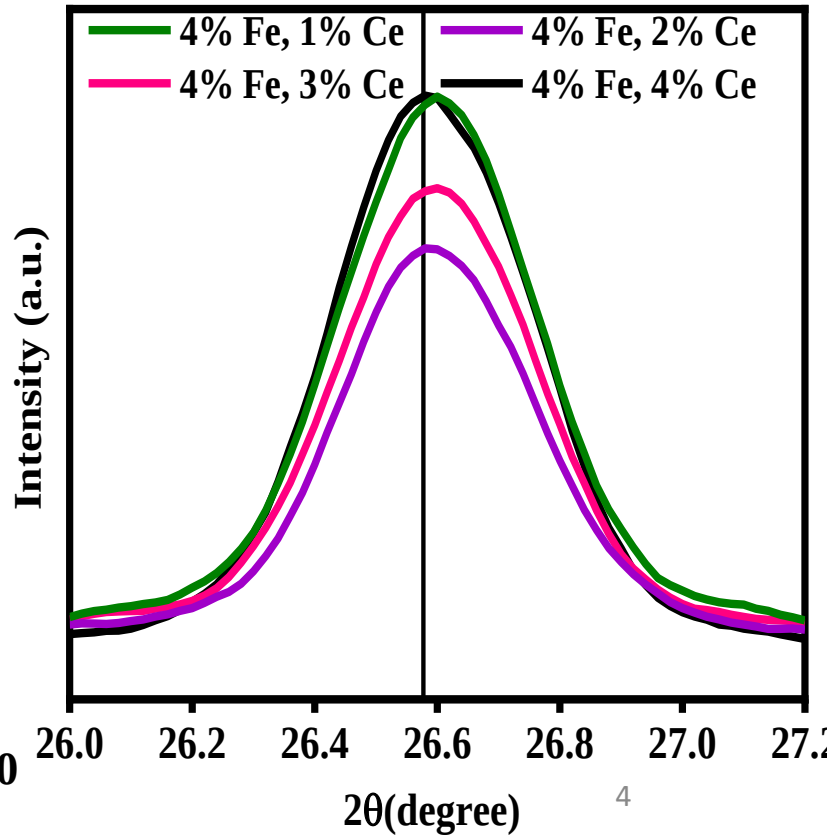

WH PLOTS

The Williamson-Hall equation:

$$\boldsymbol{\beta cos\theta = \frac{k\lambda}{D_{WH}} + 4\eta\, sin\theta}$$

where λ is the X-ray wavelength (1.54059 Å), k is the shape factor (0.9), D_{WH} is the average crystallite size, θ is the Bragg's diffraction angle, and η is the lattice strain.

Calculated Crystallite size : 18nm-20nm

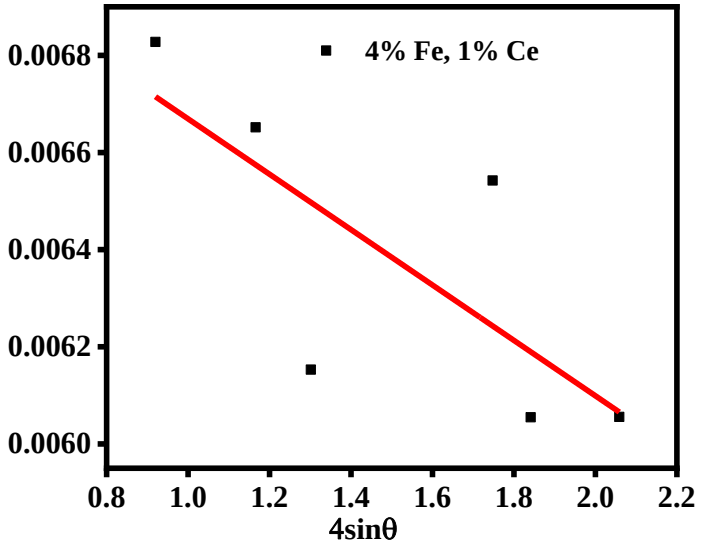

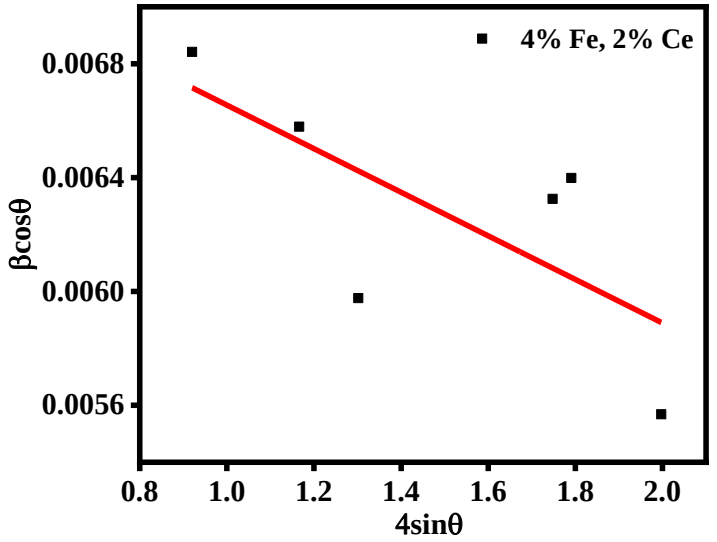

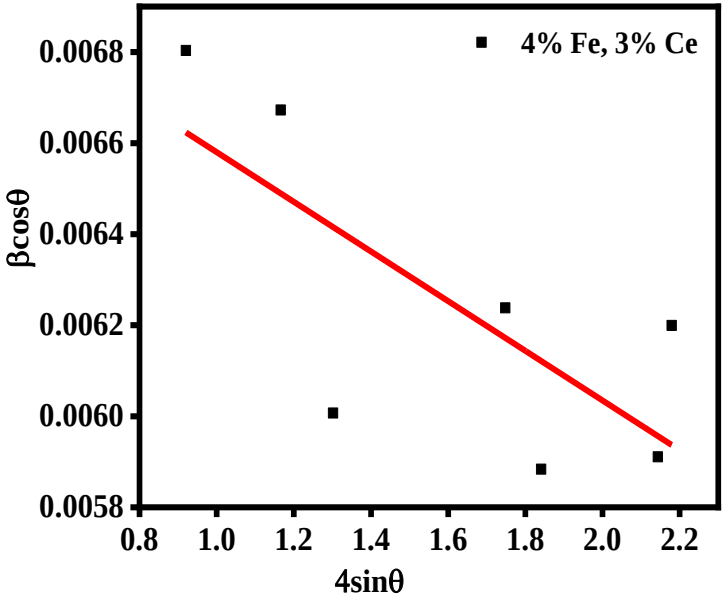

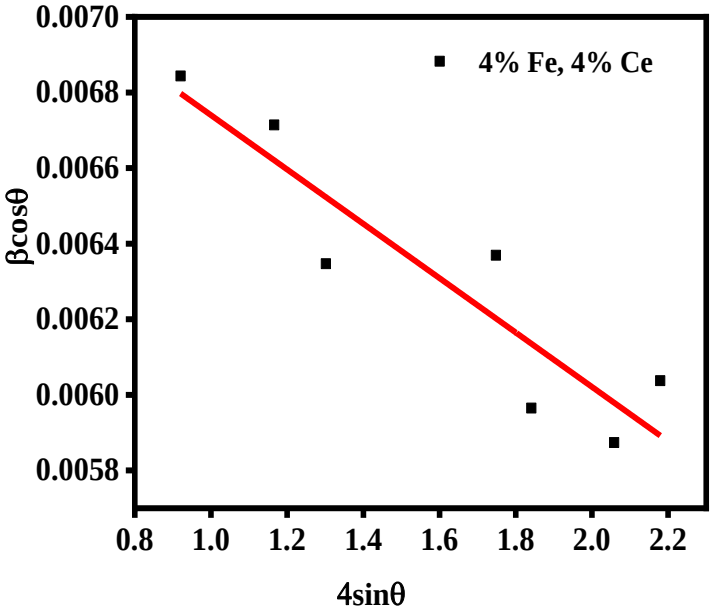

Dielectric Constant

The dielectric constant of the pelletized sample is given by

$$\varepsilon_r = \frac{C_p dl}{\varepsilon_o A}$$

where C_p, dl, A and ε_o represent the capacitance , thickness of the pelletized sample, area of cross-section of the pellet and permittivity of free space (~ 8.859×10^{-12} farad/m) respectively.

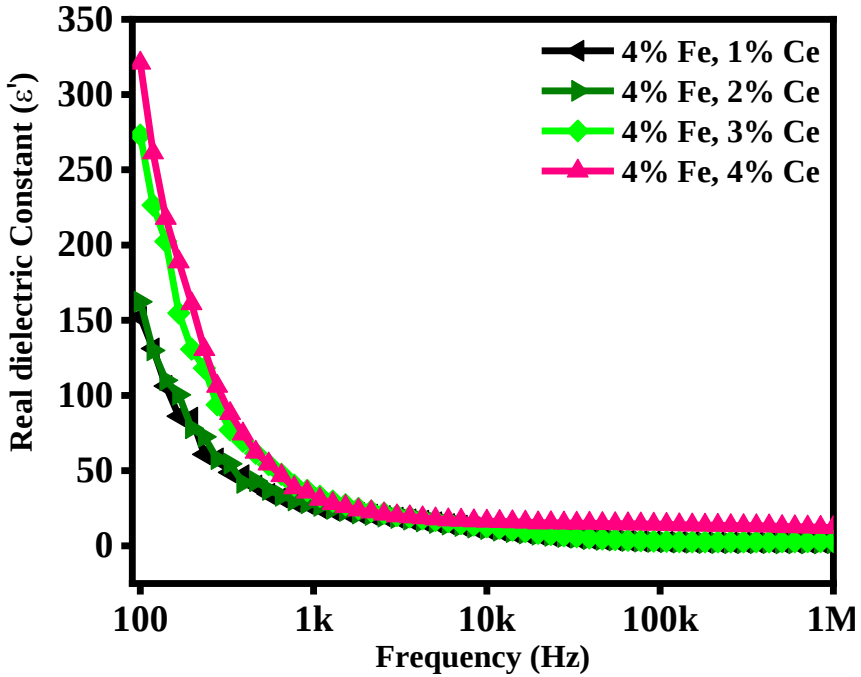

- The dielectric constant decreases rapidly with frequency up to 10^3 Hz and then stabilizes, showing dielectric dispersion.
- The dielectric dispersion is explained by Maxwell–Wagner interfacial polarization and Koop's model.
- With increasing frequency, contributions from electronic, ionic, space charge, and rotational polarizations decline as carriers fail to follow the applied field.
- Grain boundaries act as resistive regions, causing reduced dielectric constant and loss at higher frequencies.
- At high frequencies, grain boundary effects dominate due to defects, impurities, and thermally activated charge carriers, enhancing interfacial polarization.

Dielectric Constant

Havriliak Negami function in complex dielectric constant:

$$\varepsilon^* = \varepsilon_\infty + \frac{\varepsilon_s - \varepsilon_\infty}{((1+i\omega\tau_0)^{1-\alpha})^\beta} \quad (16)$$

where, ε_∞ , ε_s,ω, τ_0 represent the high frequencies dielectric constant, low frequencies electrostatic dielectric constant, angular frequency of applied electric field and relaxation time, respectively.

Table. Parameters of Havriliak–Negami (HN) function fitting

Samples Name	ε	τ_0(s)	α	β
4%Fe, 1%Ce	140.15	0.0017	0.312	0.827
4%Fe, 2%Ce	150.01	0.0014	0.359	0.712
4%Fe, 3%Ce	230.43	0.0034	0.717	0.448
4%Fe, 4%Ce	320.18	0.0038	0.760	0.266

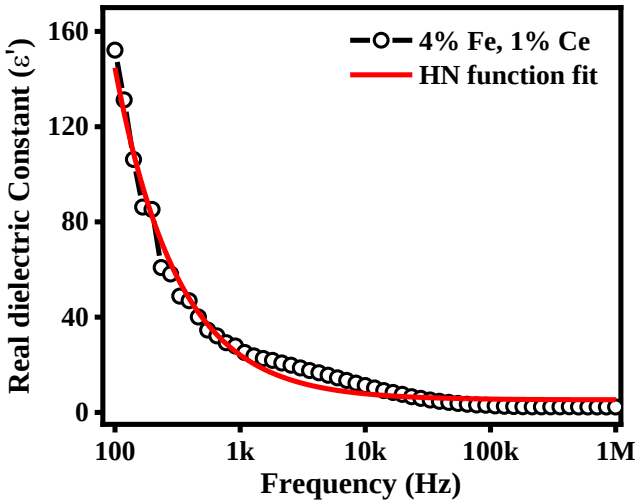

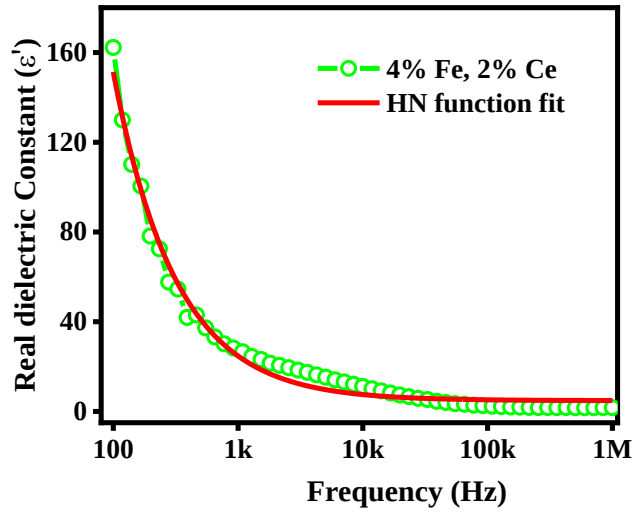

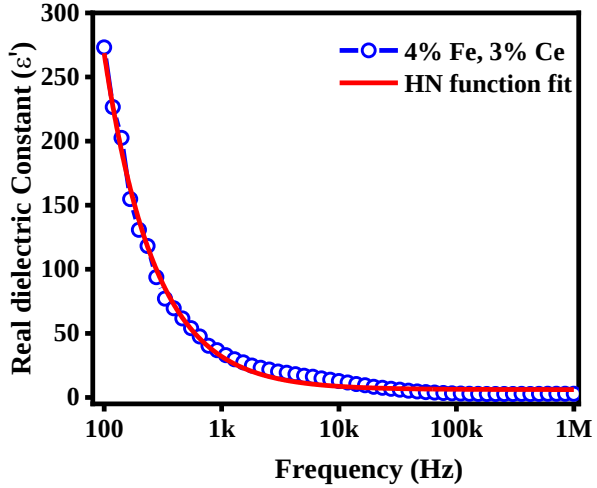

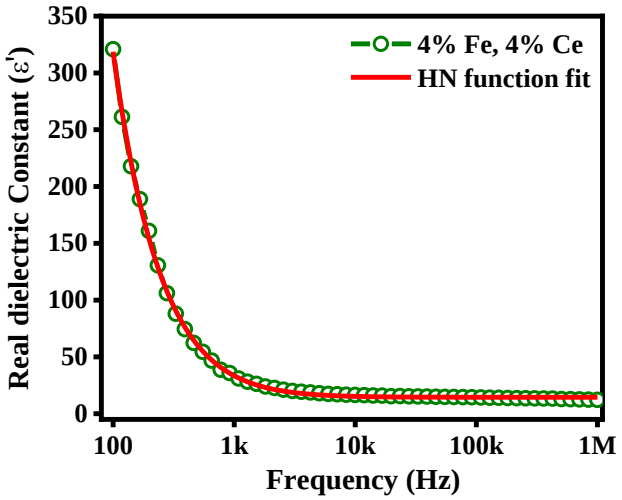

Dielectric Loss

- At higher frequencies, the charge carriers are unable to respond the oscillations of the external field, and the dielectric response becomes nearly independent of frequency.
- The presence of a relaxation peak is evident in the dielectric loss curve in all the Fe-Ce co-doped SnO_2 compounds.
- The relaxation peaks shifted to the higher frequency region.
- Such effects are likely caused by the higher density of defect states and oxygen vacancies introduced by the substitution of Fe^{3+} and Ce^{3+}/Ce^{4+} ions at Sn^{4+} sites.

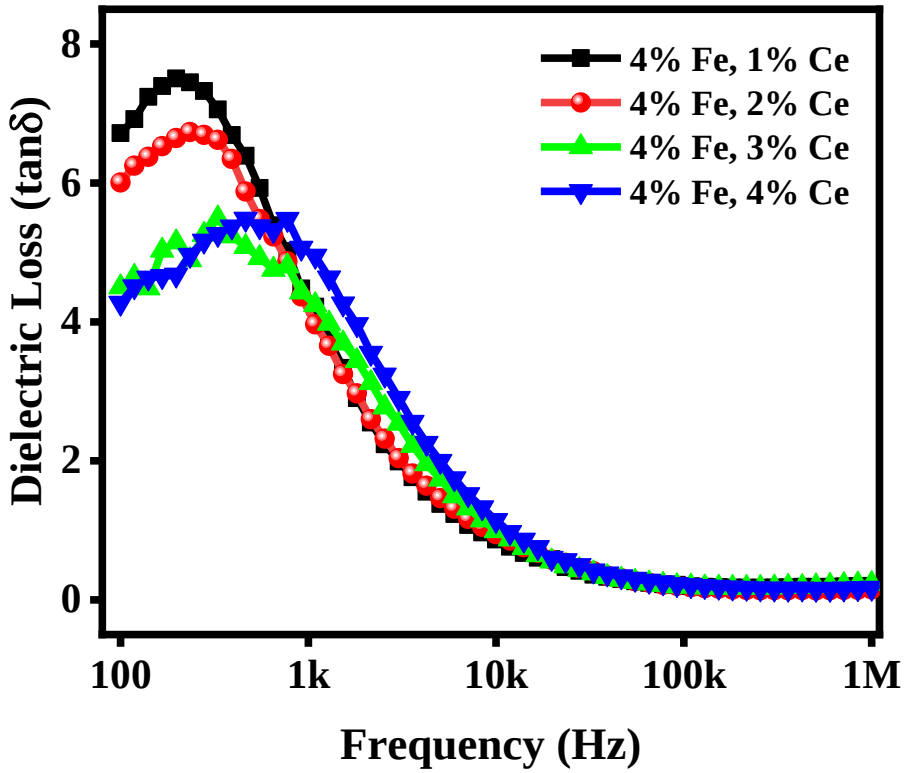

AC Conductivity Analysis

- The AC conductivity exhibits two regions: (a) a frequency independent plateau related to DC conductivity (σ_{DC}) at low frequency, which is almost constant, and (b) a frequency-dependent dispersion at high frequency attributed to AC conductivity σ_{AC}.
-
- The σ_{AC} is observed to increase with rise in frequency. The electrical conduction mechanism in pure and (Fe, Ce) co-doped SnO_2 can be attributed to the electron hopping between $Sn^{3+} \Leftrightarrow Sn^{4+}$, and $Ce^{3+} \Leftrightarrow Ce^{4+}$.

- The higher frequency promotes the charge carriers' hopping, which in turn increases the conductivity of the material.

- In addition, the substitution of Fe^{3+} at Sn^{4+} creates oxygen vacancies, which then enhances the hopping of electrons and conductivity.

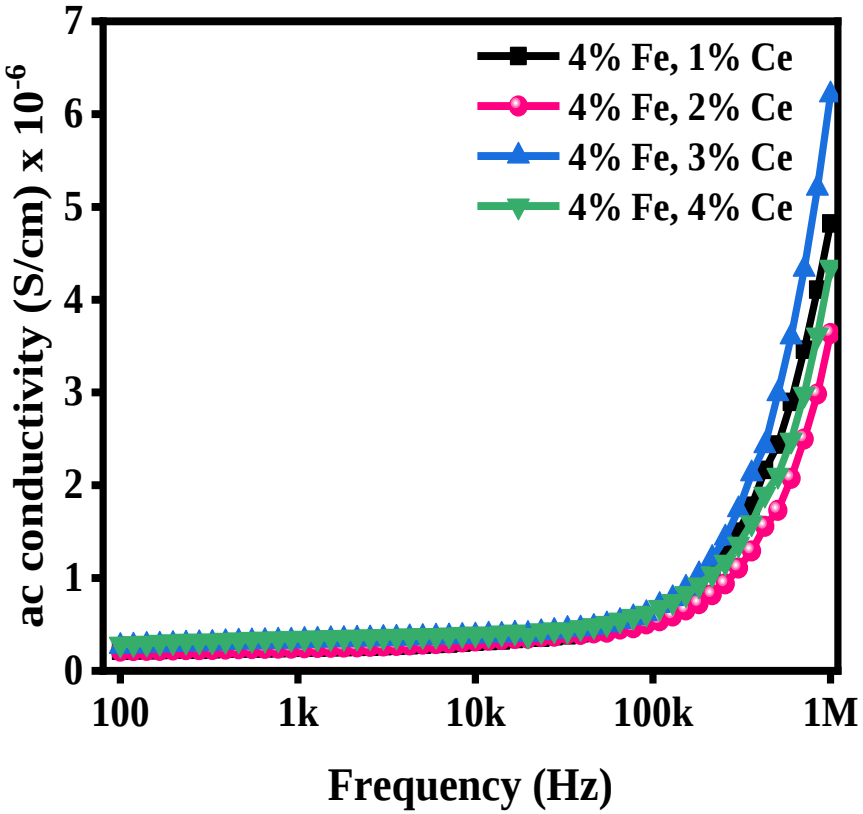

The electrical conductivity of the sample can be described by Jonscher's universal power law with the following relation:

$$\sigma_{AC}(\omega) = \sigma_{DC} + A\omega^{n}$$

where σ_{DC} denotes the frequency independent dc conductivity, A is the temperature dependent parameter, and n $(0 < n < 1)$ is the frequency exponent of the power law

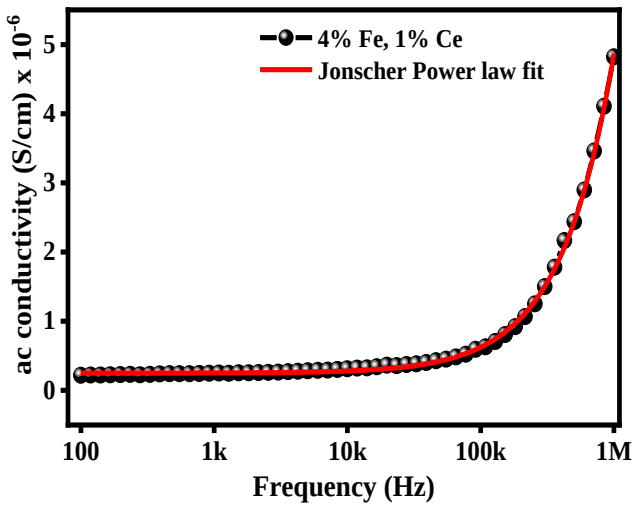

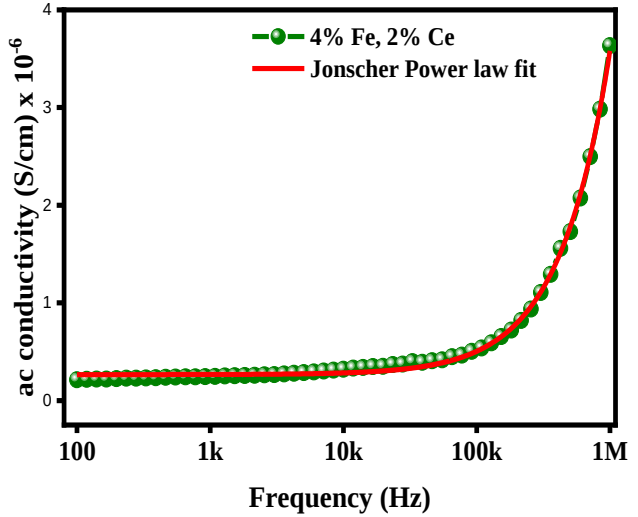

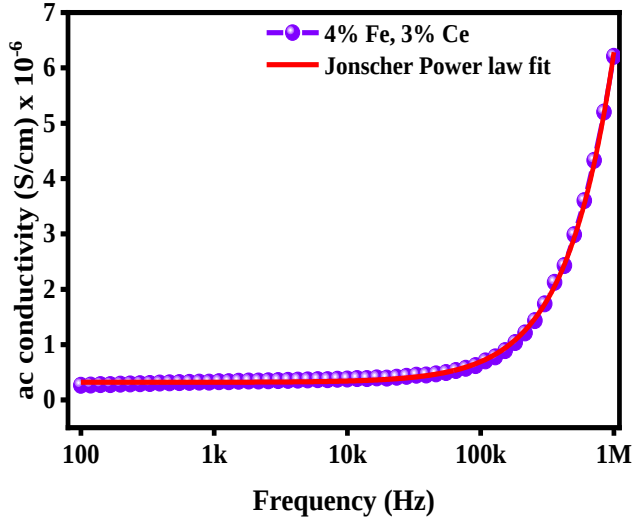

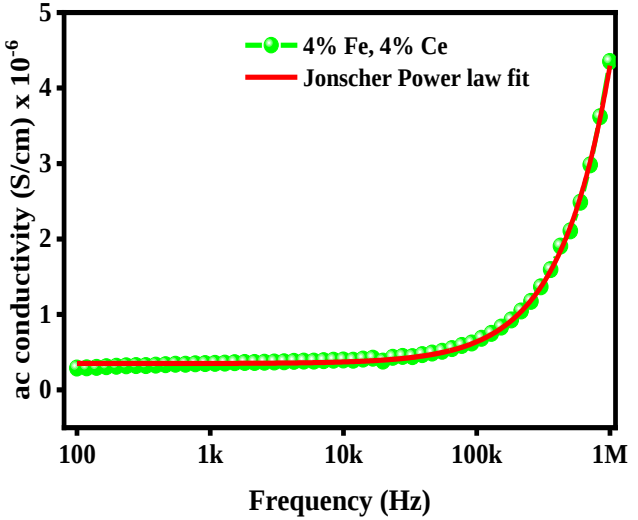

- n values exceeds the conventional range associated with Jonscher universal power law, which signifies that the electrical conduction mechanism is governed by hopping of charge carriers.
- The decrease in σ_{DC} and variation in A further indicates the incorporation of defect states induced by Ce-Fe co-doping and localised traps that facilitate frequency-dependent hopping conduction.

Table . Jonscher power law fitting parameters of AC conductivity (σ) as a function of frequency

Samples Name	σ_{dc} ($\times 10^{-6}$ Scm^{-1})	A	n	R^2
4%Fe, 1%Ce	2.5	1.3×10^{-13}	1.09	0.99896
4%Fe, 2%Ce	0.26	$4.66\times10^{-13}3$	1.14	0.99925
4%Fe, 3%Ce	0.319	3.5×10^{-13}	1.2	0.99919
4%Fe, 4%Ce	0.34	5.96×10^{-13}	1.13	0.99952

Conclusion

- XRD confirmed tetragonal rutile structure of SnO_2.
- Average crystallite size calculated using Scherrer's equation is found to increase in co-doped sample.
- Dielectric measurements showed an enhanced dielectric constant with reduced dielectric loss, explained by interfacial polarisation under the Maxwell-Wagner model and well fitted by the Havriliak-Negami model.
-
- The ac conductivity obeyed Jonscher's power law, indicating that the charge transport occurs via a hopping mechanism between different defects.

REFERENCES

Y. Kumar, H.S. Akkera, G.S. Reddy, N. Kambhala, Sol-gel spin-coated Y-doped SnO2 nanostructured thin films for various optoelectronic device applications, Phys. B Condens. Matter 683 (2024) 415881. https://doi.org/10.1016/j.physb.2024.415881.

[2] C.H. Yadav, J. Gajendiran, S. Gnanam, J.R. Ramya, S. Monisha, S. Selvalakshmi, K. Ramachandran, S.G. Raj, G.R. Kumar, Structural and magnetic properties of tin oxide (SnO2) nanoparticles for testing spintronic device applications, Mater. Lett. 358 (2024) 135863. https://doi.org/10.1016/j.matlet.2023.135863.

[3] N. Aggarwal, P. Patial, N. Rani, R.S. Panwar, A. Kapoor, S. Singla, P. Puri, K. Ravi, N. Kumar, Tailoring Structural, Microstructural, Dielectric and Gas Sensing Properties of SnO_2 Nanoparticles: Size Matters, ECS J. Solid State Sci. Technol. 14 (2025) 013007. https://doi.org/10.1149/2162-8777/ada7a1.

[4] C. Wang, Y. Jiang, L. Liu, J. Yan, J. Luo, Z. Yang, X. Shi, X. Lu, J.-M. Liu, G. Zhou, J. Gao, Low acidic SnO2 precursor for efficient flexible perovskite solar cells, Surf. Interfaces 72 (2025) 107041. https://doi.org/10.1016/j.surfin.2025.107041.

[5] M. Periyasamy, S.K. Saha, V. Balamurugan, U. Sengupta, S. Sain, C. Pichandi, M. Sudharsan Natteri, A. Kar, Tuning the structural and optical properties of SnO2 nanocrystals through flow conditions in a continuous flow microreactor, J. Ind. Eng. Chem. 151 (2025) 264–275. https://doi.org/10.1016/j.jiec.2025.03.052.

[6] A. Ahmed, M.N. Siddique, T. Ali, P. Tripathi, Defect assisted improved room temperature ferromagnetism in Ce doped SnO2 nanoparticles, Appl. Surf. Sci. 483 (2019) 463–471. https://doi.org/10.1016/j.apsusc.2019.03.209.

[7] E. Anuja, I. Potheher, M. Meena, M. Vimalan, Impact on bandgap, electrical and magnetic properties of SnO2 nanoparticles by cerium and samarium, J. Mol. Struct. 1320 (2025) 139617. https://doi.org/10.1016/j.molstruc.2024.139617.

[8] V. Agrahari, M.C. Mathpal, S. Kumar, M. Kumar, A. Agarwal, Cr modified Raman, optical band gap and magnetic properties of SnO2 nanoparticles, J. Mater. Sci. Mater. Electron. 27 (2016) 6020–6029. https://doi.org/10.1007/s10854-016-4525-2.

[9] N. Bhakta, P.K. Chakrabarti, XRD analysis, Raman, AC conductivity and dielectric properties of Co and Mn co-doped SnO2 nanoparticles, Appl. Phys. A 125 (2019) 73. https://doi.org/10.1007/s00339-018-2370-2.

[10] H.R. Khakhal, S. Kumar, D. Patidar, S. Kumar, V.S. Vats, B. Dalela, P.A. Alvi, N.S. Leel, S. Dalela, Correlation of oxygen defects, oxide-ion conductivity and dielectric relaxation to electronic structure and room temperature ferromagnetic properties of Yb3+ doped CeO2 nanoparticles, Mater. Sci. Eng. B 297 (2023) 116675. https://doi.org/10.1016/j.mseb.2023.116675.

[11] T.H. Li, L.Z. Liu, X.X. Li, X.L. Wu, H.T. Chen, P.K. Chu, Oxygen vacancy density-dependent transformation from infrared to Raman active vibration mode in SnO_2 nanostructures, Opt. Lett. 36 (2011) 4296. https://doi.org/10.1364/OL.36.004296.

THANK YOU